Progress In Electromagnetics Research M, Vol. 60, 179–188, 2017

Compact Microstrip Lowpass Filter with High and Wide Rejection in the Stopband Utilizing Flabelliform Resonators

Ashkan Abdipour* and Arash Abdipour

Abstract—In this paper, a microstrip lowpass filter with −3 dB cutoff frequency of 3.8 GHz consisting of two cascaded resonators with flabelliform patches and two symmetric suppressing cells is proposed. To design the filter, the impact of each transmission line on the frequency response is determined by extracting the equations of the insertion loss (S_{21}) and return loss (S_{11}) on the basis of the equivalent LC circuit of the main resonance cell and the cascaded structure. The designed filter is constructed and tested, and a good agreement between the results of simulation and measurement is obtained. In the whole stopband region, a return loss close to zero and an acceptable suppression level of −30 dB from 4.47 to 25.17 GHz are achieved. Furthermore, a flat insertion loss in the passband and a low return loss (−23.02 dB) in this band can prove desired in-band and out-band frequency response.

1. INTRODUCTION

Microstrip lowpass filters (LPFs) are one of the most important components that have been utilized widely in wireless communication systems and played a key role for many years. So far, several compact LPFs have been proposed to achieve desired frequency response such as wide stopband with high rejection level and sharp roll-off. For example, in [1], a microstrip lowpass filter with quasi-elliptic response using both loaded radial-shape patches and meandered main transmission line is proposed. However, it suffers from a gradual transition band and low level of stopband rejection. To expand the stopband region in the frequency response of LPFs, hairpin resonators can be useful [2–6]. By utilizing this unit in [2], the stopband is expanded. However, the overall circuit size is relatively large, and the skirt performance is not desired. A method to design an LPF with wide stopband uses stepped impedance hairpin resonators with radial stubs, done in [3], but this design is not successful in achieving a sharp roll-off rate. In [4], by employing stepped impedance hairpin units a compact LPF is proposed. However, this filter has a narrow stopband. In [5], another method to propose an LPF based on an application of shunt open-stubs coupled-line in the structure of hairpin unit is introduced, although the designed filter has a gradual transition band and large circuit size. In [6], defected ground structure (DGS) as a popular method is applied to design an LPF with sharp rejection. However, the proposed circuit using DGS method cannot be utilized on metal surfaces. To design an LPF, rat-race directional couplers are used to operate as bandstop transversal filtering sections (TFSs), in [7]. However, by adopting this method the occupied area is significantly increased, and the rejection band is also not wide enough. In [8], an LPF with enhanced performance on the basis of strong slow-wave effects is developed, but the circuit is complex, and the filter has high insertion loss in the passband. A microstrip LPF by using triangular and radial patch resonators is designed [9]; however, this filter suffers from gradual transition band. Another technique to design an LPF with sharp transition band uses asymmetric high-low impedance patches, which is reported in [10]. To design an LPF with wide stopband, a cascaded microstrip coupled-line hairpin unit and semi-circle stepped-impedance shunt stubs

Received 28 July 2017, Accepted 14 July 2017, Scheduled 4 October 2017
* Corresponding author: Ashkan Abdipour (Ashkan_Abdipour@yahoo.com).
The authors are with the Young Researchers and Elite Club, Kermanshah Branch, Islamic Azad University, Kermanshah, Iran.

are used in [11]. In [12], by employing LC resonant structures and transformed radial stubs an LPF is proposed. One more approach to design an LPF with sharp transition band uses LC tank resonators, which is reported in [13]. However, the occupied area of circuits, [11–13], are relatively large. In [14], a lowpass filter using polygon patch resonant cells, T-shaped resonators and two different suppressing cells is designed; however, this filter does not have a sharp transition band. Another method to design an LPF with acceptable frequency response is cascading resonators with polygon patches [15], but it has a large circuit size. In this paper, a lowpass filter (LPF) with −3 dB cutoff frequency located at 3.8 GHz is proposed. The designed LPF is composed of two main resonators with flabelliform patches and two symmetric suppressing cells having the same structure to omit the aforementioned defects of the frequency response in the stopband region.

2. FILTER STRUCTURE AND ANALYSIS

2.1. The Primary Resonator Structure

The configuration of the primary resonator using flabelliform patch with −3 dB cutoff frequency of 4.15 GHz and its equivalent LC circuit are illustrated in Fig. 1(a). As observed, low impedance flabelliform patch and high impedance transmission line are modeled by a capacitance ($C1$) and an inductor ($L1$), respectively. $L2$ accounts for the transmission lines determined by Lb in Fig. 1(a). $C2$, $C3$ and $C4$ model the capacitance between the microstrip structure and the ground. The values of the lumped elements of the proposed resonator are as follows [16]: $L1 = 1.467$ nH, $C1 = 0.661$ pF, $L2 = 1.367$ nH, $C2 = 0.091$ pF and $C3 = C4 = 0.059$ pF. Note that the values of inductors and capacitances are obtained based on an RO4003 substrate with a thickness of 0.508 mm and permittivity of 338. Fig. 1(c) shows the EM simulation and frequency response of LC circuit, which are in good agreement. According to the depicted frequency response of the primary resonator in Fig. 1(b), the return loss and insertion loss in the passband are better than 20 and 0.1 dB, respectively. Furthermore, the primary resonance cell creates a transition zero at 5.078 GHz with an attenuation level of −36.751 dB bringing about a suppressing band of −8.2 dB from 6.875 to 16.85 GHz.

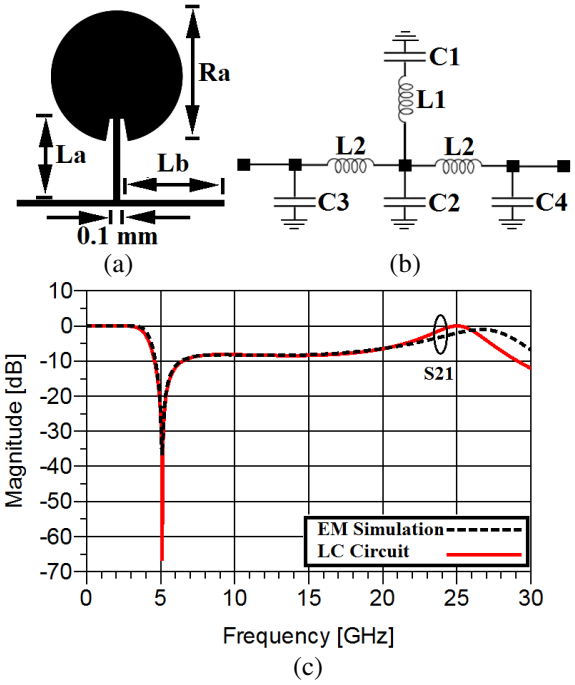

Figure 1. (a) The configuration of the primary resonator with flabelliform patch. (b) The equivalent LC circuit of the primary resonator. (c) The EM simulation result and the frequency response of LC circuit of the primary structure.

As observed, the primary resonator suffers from a gradual roll-off rate and also a low level of suppression in the stopband.

2.2. The Main Resonator Structure and Analysis

The configuration of the main resonator employing two primary resonators which are placed symmetrically around X-axis and its equivalent LC circuit is illustrated in Figs. 2(a) and (b), respectively. To find which variables can affect the frequency response and in particular the location of the transmission zero, the equations of insertion loss (S'_{21}) and return loss (S'_{11}) of the main resonator shown in Fig. 2(a) on the basis of its LC circuit are obtained as follows:

$$S'_{11} = \frac{\left(2tx's + y't^2s^2 - y'Z_0^2\right)}{\left(2Z_0x' + 2Z_0ty's + 2tx's + y't^2s^2 + y'Z_0^2\right)} \tag{1}$$

$$S'_{21} = \frac{\left(2Z_0x'\right)}{\left(2Z_0x' + 2Z_0ty's + 2tx's + y't^2s^2 + y'Z_0^2\right)} \tag{2}$$

where

$$x' = \left(1 + wqs^2\right) \tag{3}$$

$$y' = \left[\left(1 + wqhs^2\right) + (h + 2q)\, s\right] \tag{4}$$

Clearly, the insertion loss and return loss of this resonator can be controlled by changing the values of m' and n'. In order to illustrate how changing these variables can affect the frequency response, several full-wave simulations versus changing their corresponding microstrip realizations, i.e., $L'1$, R' and θ' are plotted in Figs. 3(a), (b) and (c), respectively. In this case the remaining parameters in Fig. 2(a) are kept constant.

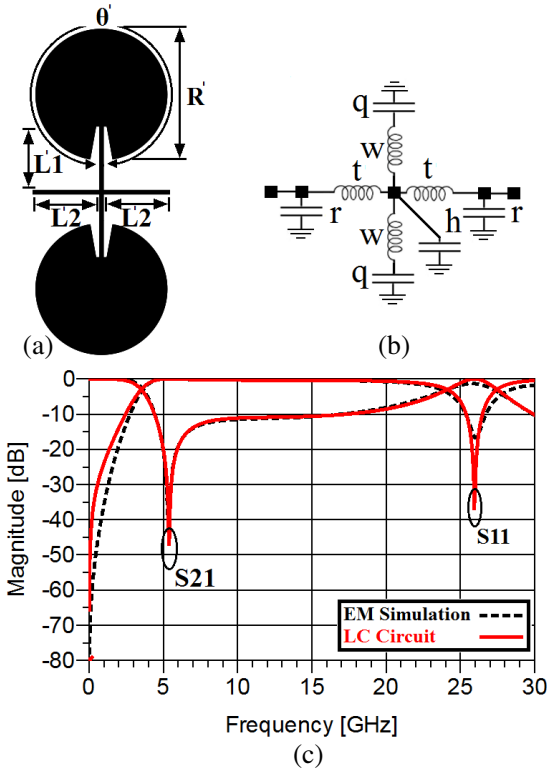

Figure 2. (a) The configuration of the main resonator with two flabelliform patches. (b) The equivalent LC circuit of the main resonator with two flabelliform patches. (c) The EM simulation result and the frequency response of LC circuit of the main structure.

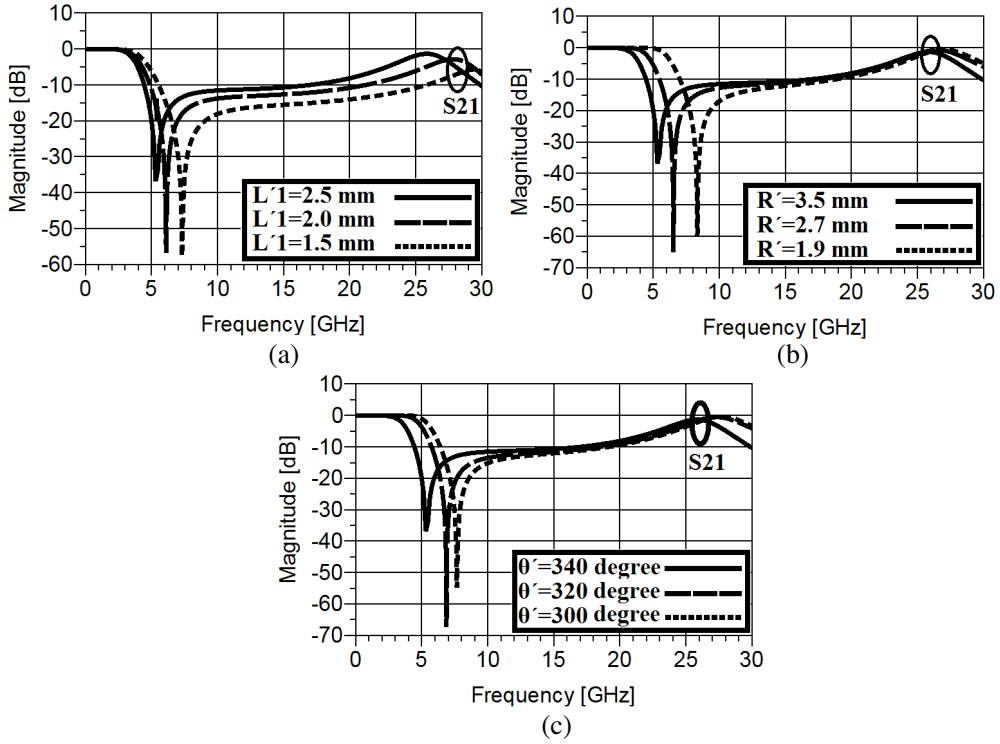

Figure 3. The behavior of the main resonator against changing the values of $L'1$, R' and θ'.

As can be seen from Fig. 3(a), by increasing the value of $L'1$ from 1.5 to 2.5 mm with steps of 0.5, the transition zero at 5.313 GHz will move to lower frequencies causing a sharper transition band. As observed, decreasing the value of $L'1$ does not affect the return loss in the passpand significantly. Moreover, changing the value of θ' from 300 to 340 degrees with steps of 20 degrees and also the value of R' from 1.9 to 3.5 with steps of 0.8, both the mentioned TZ and -3 dB cutoff frequency will move toward lower frequencies. Obviously, increasing the mentioned variables, i.e., θ' and R', leads to decreasing the level of return loss in the passband, and consequently a better in-band performance can be obtained. Finally, the main resonator with -3 dB cutoff frequency of 3.652 GHz is designed. According to the depicted EM simulation result in Fig. 2(c), the stopband of the main resonator can suppress a frequency range from 4.13 up to 19.04 GHz with a suppressing level of -10 dB. Moreover, this resonator creates a transition zero (TZ) at 5.313 GHz with corresponding attenuation level of -42.978 dB creating a roll-off rate equal to 22.45 dB/GHz. The correlative parameters in Fig. 2(a) are: $L'1 = 2.5$ mm, $L'2 = 1.85$ mm, $R' = 3.5$ mm and $\theta' = 340$ degrees. The values of lumped elements of the shown equivalent LC in Fig. 2(b) are [16]: $r = 0.029$ pF, $h = 0.112$ pF, $t = 1.277$ nH, $q = 0.591$ pH, $w = 1.477$ nH.

2.3. The Cascaded Structure and Analysis

Connecting two of the main resonators with different dimensions in series leads to creating another TZ.

More TZs results in expanding the stopband with an improved suppression level and better skirt performance. Therefore, to widen the stopband and improve the transition band of the illustrated resonator in Fig. 2(a), the final cascaded lowpass resonator employing two of the main resonators with different dimensions is designed. The configurations of the connected resonators in series and its equivalent LC circuit are shown in Figs. 4(a), and (b), respectively. As mentioned, calculating insertion loss (S_{21}) and return loss (S_{11}) according to the equivalent LC circuits can determine the role of each section of the resonators on the frequency response. Thus, the equations of S_{21} and S_{11} based on the shown equivalent LC circuits of the shown cascaded lowpass resonator in Fig. 4(a) are extracted as

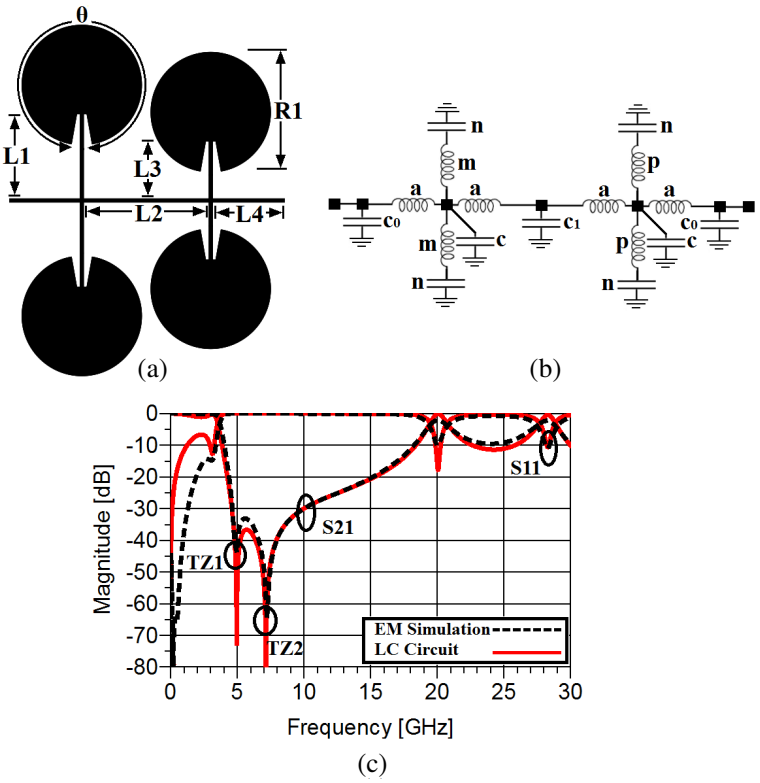

Figure 4. (a) The configuration of the cascaded resonator employing two of the main resonators with different dimensions. (b) The lumped circuit of the cascaded resonator. (c) The EM simulation and the frequency response of the lumped circuit of the final cascaded resonator.

follows:

$$S_{11} = \frac{\left(4Z_O^2x^2B^{'2}A'' + A'B'B''D'^2 - A'^2D'^2A''\right)}{B'\left(B'B''D'^2 - A'A''D'^2\right)} \tag{5}$$

$$S_{21} = \frac{8Z_O^3u^2xB'B''}{1 - A'A''D'D''} \tag{6}$$

Where

$$A' = 2axs + ya^2s^2 - yZ_O^2 \tag{7}$$

$$D' = B' = 2axs + ya^2s^2 + 2Z_Ox + 2Z_Oays + yZ_O^2 \tag{8}$$

$$A'' = 2aus + wa^2s^2 - wZ_O^2 \tag{9}$$

$$D'' = B'' = 2aus + wa^2s^2 + 2Z_Ou + 2Z_Oaws + wZ_O^2 \tag{10}$$

$$x = \left(1 + mns^2\right) \tag{11}$$

$$y = \left[\left(1 + mncs^3\right) + (c + 2n)\, s\right] \tag{12}$$

$$u = \left(1 + pns^2\right) \tag{13}$$

$$w = \left[\left(1 + pncs^3\right) + (c + 2n)\, s\right] \tag{14}$$

In order to illustrate how the calculated equations, i.e., S_{21} and S_{11}, can be influenced by changing the values of the main lumped parameters, several frequency responses versus (n), (m) and (p) are plotted in Figs. 5(a), (b), and (c), respectively.

In these cases, the remaining parameters of the shown equivalent LC circuit in Fig. 4(a) are kept constant. As observed from Fig. 5(a), the operating frequency of the proposed LPF can be controlled

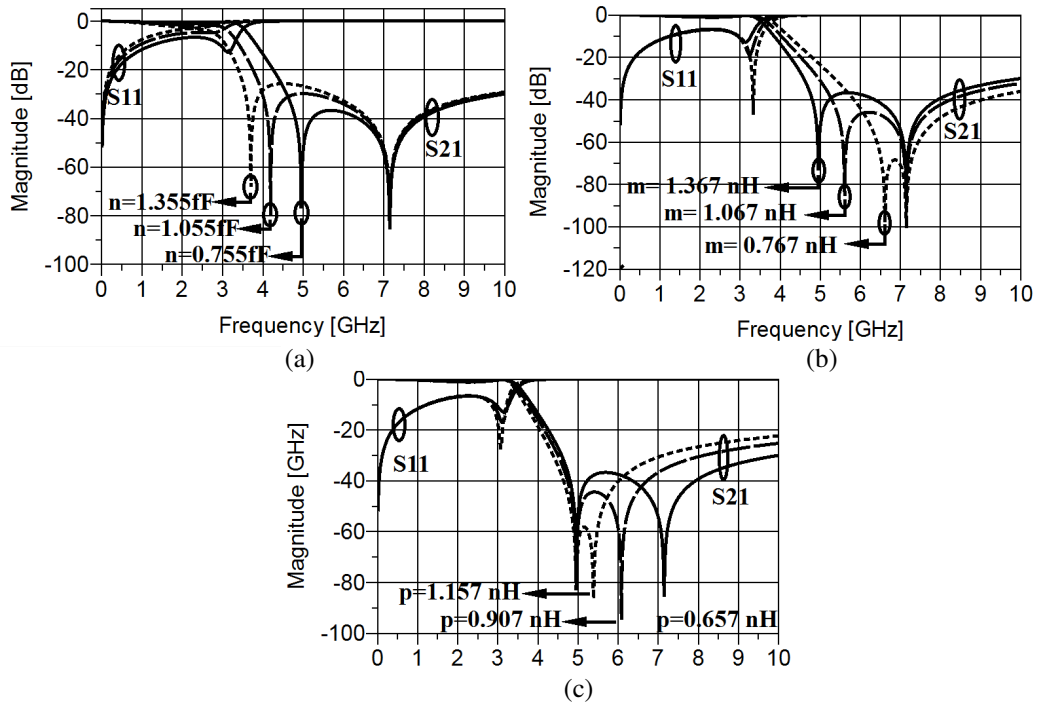

Figure 5. The calculated frequency response. (a) Versus changing the value of (n). (b) Versus changing the value of (m). (c) Versus changing the value of (p).

by changing the value of (n). By increasing the value of this capacitance from 0.755 fF to 1.355 fF with steps of 0.3, both the first transition zero at 4.950 GHz and -3 dB cutoff frequency move toward lower frequency. Moreover, to have better return loss, smaller value of (n) can be chosen. As shown in Fig. 5(b), decreasing the value of the determined inductor by (m) from 1.367 nH to 0.767 nH with steps of 0.3 makes the skirt performance gradual without affecting the operating frequency or return loss. According to Fig. 5(c), by decreasing the value of (p) from 1.157 nH to 0.657 nH with steps of 0.25, the second transition zero (TZ2) moves toward higher frequencies and expands the rejection band with an acceptable suppression level, but there is no noticeable effect on return loss. Eventually, a cascaded resonator with acceptable frequency response is obtained. The correlative dimensions in Fig. 4(a) are: $L1 = 2.5$ mm, $L2 = 3.8$ mm, $L3 = 1.7$ mm, $L4 = 1.8$ mm, $R = 3.5$ mm and $\theta = 340$ degrees. The values of inductors and capacitors of the shown equivalent LC in Fig. 4(a) are [16]: $C0 = 0.043$ pF, $C1 = 0.07$ pF, $C = 0.08$ pF, $a = 1.067$ nH, $n = 0.755$ pH, $m = 1.367$ nH and $p = 0.655$ nH. As shown in Fig. 4(c), the proposed cascaded resonator has two TZs at 4.907 GHz (TZ1) and 7.222 GHz (TZ2) with attenuation levels of -51.421 and -65.957 dB, respectively. Compared with the shown frequency response of the main resonator in Fig. 2(b), the stopband is improved, and the spurious frequencies from 4.367 GHz up to 15.47 GHz are suppressed with a rejection level of -20 dB. The -3 dB operating frequency is partially affected and shifted to 3.692 GHz which is trivial in comparison to the cutoff frequency of the shown resonator in Fig. 2(a). Moreover, the first TZ (TZ1) at 4.907 GHz is located close to the operating frequency leading to a desired transition band from 3.692 to 4.78 GHz with corresponding levels of -3 and -40 dB, respectively.

As observed from the EM simulation result in Fig. 4(b), the cascaded resonator suffers from a narrow stopband.

2.4. The Employed Suppressing Cells Structure and The Final Filter Design

To expand the rejection band and improve the suppression level, two symmetric suppressing cells are presented. The schematic of the designed suppressing unit, its equivalent LC circuit and its frequency response are illustrated in Fig. 6, respectively. As observed from Fig. 6(b), the inductances $Ls1$ and

$Ls2$ account for the transmission lines determined by $TL1$, and also $Ls3$ and $Ls4$ model the shown transmission lines by $TL3$ and $TL2$ in Fig. 6(a). The low-impedance transmission line is modeled by ($Cs1$). Cps, $C0s$, $C2s$ and $C3s$ present the capacitance between the microstrip structure and the ground. The coupling effect caused by the shown gap in Fig. 6(a) is modeled by Cg. The values of inductors and capacitors of the shown equivalent LC in Fig. 6(b) are [16]: $Ls1 = 9.5$ nH, $Ls2 = 6.859$ nH, $Ls3 = 0.6$ nH,

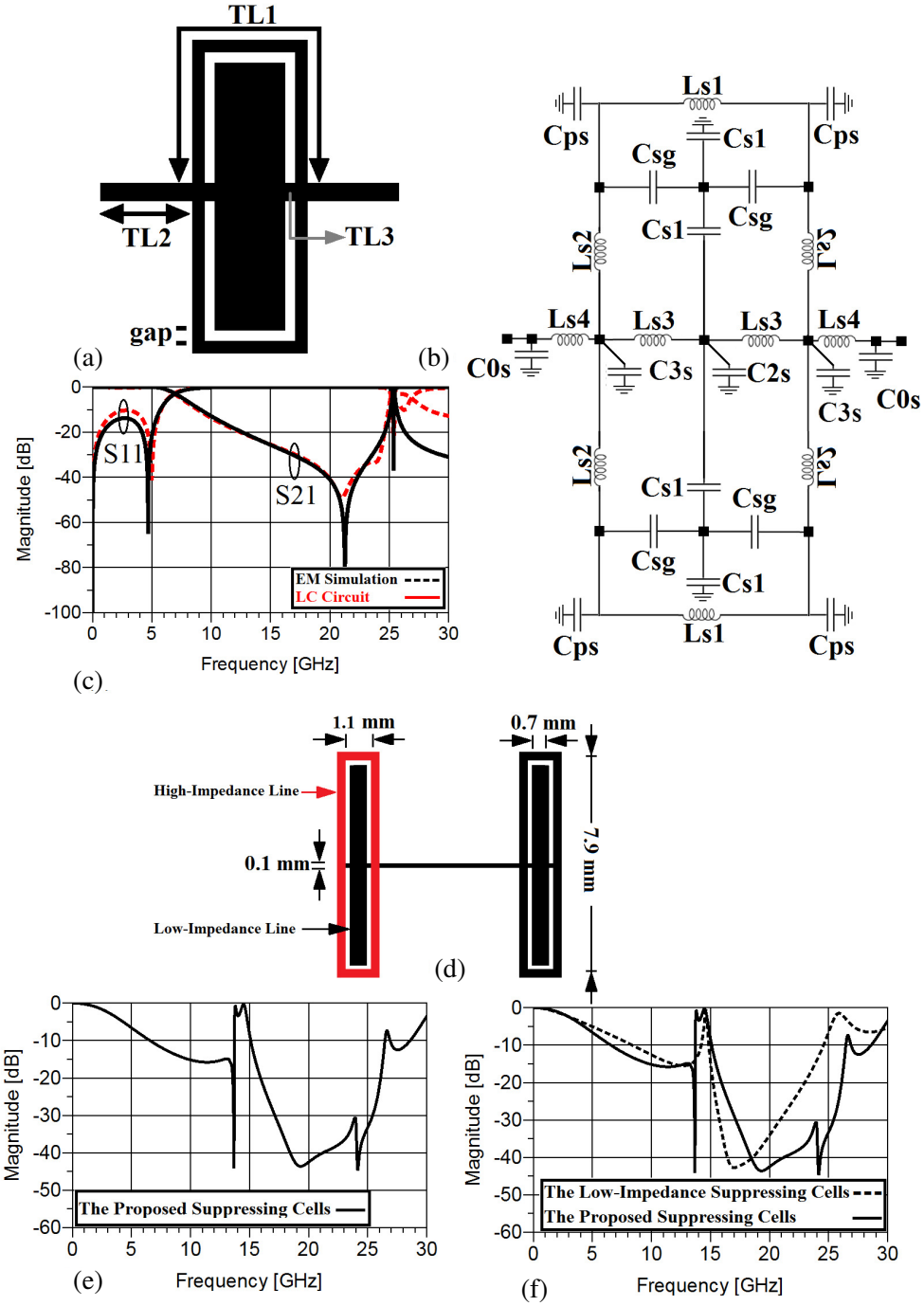

Figure 6. (a) The schematic and frequency response of the proposed suppressing cells employing two different units. (b) The frequency response of the proposed suppressing cells. (c) The frequency response of the proposed suppressing cells without its high-impedance lines.

$Ls4 = 1.2\,\text{nH}$, $Cs1 = 0.64\,\text{pF}$, $Csg = 0.011\,\text{fF}$, $Cps = 0.0051\,\text{pF}$, $C0s = 0.021\,\text{fF}$, $C2s = 0.013\,\text{fF}$, $C3s = 0.011\,\text{fF}$. As can be seen, the employed suppressing resonators consist of low-impedance lines as the main part and high-impedance lines. The comparison between the frequency responses of the suppressing cell with and without high-impedance lines in Fig. 6(c) indicates that this resonator is not able to suppress unwanted frequencies from 20.9 GHz up to 25.89 GHz without high-impedance lines. Thus, adapting high-impedance lines can modify the performance of the mentioned resonance cell.

Finally, by applying the mentioned suppressing cells to the shown cascaded resonators in Fig. 4(a), a microstrip lowpass filter with $-3\,\text{dB}$ cutoff frequency of 3.8 GHz is designed. The configurations of the proposed structure and its frequency response are illustrated in Figs. 7(a) and (b), respectively. As can be seen, the implemented LPF has a transition zero at 4.614 GHz with corresponding attenuation level of $-67.291\,\text{dB}$, which leads to a sharp transition band.

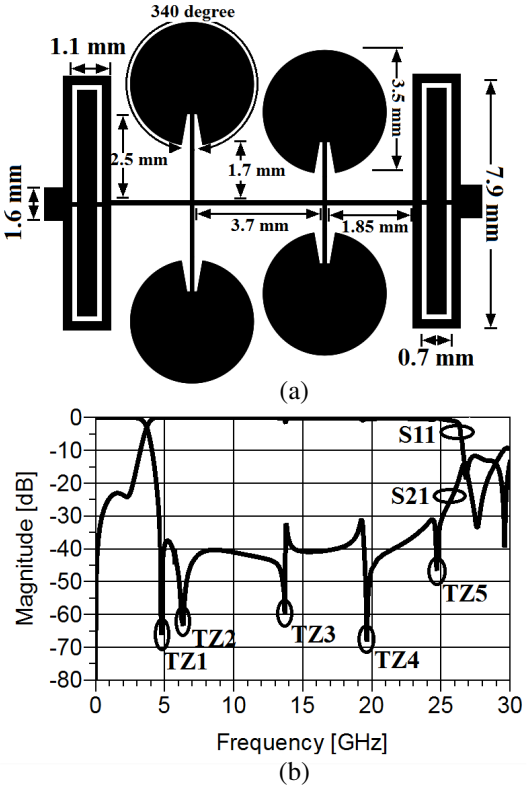

Figure 7. (a) The configuration of the proposed LPF. (b) The frequency response of the proposed LPF.

Moreover, $TZ2$, $TZ3$, $TZ4$ and $TZ5$ lead to widening the stopband bandwidth with corresponding suppression level of $-30\,\text{dB}$.

3. MEASUREMENT AND SIMULATION RESULTS

A photograph of the proposed LPF is illustrated in Fig. 8(a). The proposed LPF is designed, fabricated and tested. The implemented LPF is constructed on an RO4003 substrate with a thickness of 0.508 mm and permittivity of 32.

The simulation and measurement results of the designed LPF are carried out by using an EM-simulator ADS based on the method of moments and a HP8757A network analyzer, respectively. The simulation and measurement frequency responses of the proposed LPF are illustrated in Fig. 8(b). As can be seen, $-3\,\text{dB}$ cutoff frequency of the proposed filter is located at 3.8 GHz. According to the measurement results, in the whole passband region the insertion loss is close to zero, which shows a

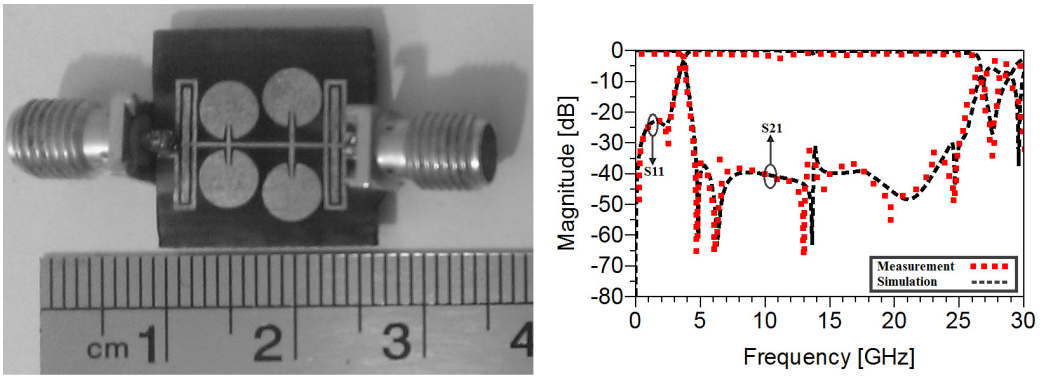

(a) (b)

Figure 8. (a) The configuration of the proposed LPF. (b) The results of simulation and measurement of the proposed LPF.

flat response, and also in this band the return loss is better than −23.05 dB. As observed, close to the operating frequency two transmission zeros (TZs) with attenuation levels of −67.286 and −65.447 exist.

Thanks to these TZs, a steep transition band from 3.8 up to 4.563 GHz with corresponding attenuation levels of −3 and 60 dB, respectively, is measured. The stopband region suppresses spurious frequencies from 4.47 to 25.17 GHz with corresponding rejection level of −30 dB. Moreover, in the rejection band a flat return loss close to zero is obtained. The occupied area of the proposed filter is about 9.8 mm × 10.3 mm. Table 1 compares the performances of the proposed lowpass filter and previous works.

Table 1. Comparison between the performance of the proposed lowpass filter and previous works.

Ref.	Return Loss (dB)	Insertion Loss (dB)	Suppression Level (dB)	Stopband Bandwidth (GHz)	Size (mm × mm)
[1]	Almost 32.5	-	15	7.04	13.2 × 13.2
[2]	14	0.45	20	8.6	0.7 × 12.9
[3]	Almost 12	0.5	10	10	10 × 10
[4]	20	0.4	20	4.12	22.4 × 24.05
[5]	16.3	0.5	20	3.8	34.62 × 70.95
[6]	Almost 25	0.5	20	6.4158	24.3 × 9.54
[7]	16.4	-	20	4.76	Very large
[8]	Almost 12	0.6	30	12.2	25 × 10
[9]	Almost 14	0.4	15	14.85	18.11 × 14.85
[10]	14.35	0.25	22	28.587	26.35 × 9.184
[11]	10	1.2	10	15	20 × 23
[15]	19.32	0.906	22	17.88	18.1 × 9.3
This Work	23.05	0.083	30	20.7	9.8 × 10.3

4. CONCLUSION

A microstrip LPF with compact size and wide stopband is designed, fabricated and measured. The simulation and measurement results are in good agreement. The proposed structure is composed of two cascaded resonators with flabelliform patches and two symmetric suppressing cells. To clarify the importance of each segment of the cascaded resonators, the equations of insertion loss and return loss based on the equivalent LC circuit are extracted and investigated in details.

REFERENCES

1. Wang, J., L. J. Xu, S. Zhao, Y. X. Guo, and W. Wu, "Compact quasi-elliptic microstrip lowpass filter with wide stopband," *IEE Electron. Lett.*, Vol. 46, No. 20, 1384–1385, 2010.
2. Luo, S., L. Zhu, and S. Sun, "Stopband-expanded low-pass filters using microstrip coupled-line hairpin units," *IEEE Microw. Wireless Compon. Lett.*, Vol. 18, No. 8, 506–508, Aug. 2008.
3. Wei, X. B., P. Wang, M. Q. Liu, and Y. Shi, "Compact wide-stopband lowpass filter using stepped impedance hairpin resonator with radial stubs," *IEE Electron. Lett.*, Vol. 47, No. 15, 862–863, Jul. 2011.
4. Li, L., Z. F. Li, and J. F. Mao, "Compact lowpass filters with sharpand expanded stopband using stepped impedance hairpin units," *IEEE Microw. Wireless Compon. Lett.*, Vol. 20, No. 6, 31–312, Jul. 2010.
5. Velidi, V. K. and S. Sanyal, "Sharp roll-off lowpass filter with wide stopband using stub-loaded coupled-line hairpin unit," *IEEE Microw. Wireless Compon. Lett.*, Vol. 21, No. 6, 301–303, Jun. 2011.
6. Mandal, M. K., P. Mondal, S. Sanyal, and A. Chakrabarty, "Low insertion-loss, sharp-rejection and compact microstrip low-pass filters," *IEEE Microw. Wirel. Compon. Lett.*, Vol. 16, No. 11, 600–602, 2006.
7. Gomez-Garcia, R., M. A. Sanchez-Soriano, M. Sanchez Renedo, G. Torregrosa-Penalva, and E. Bronchalo, "Extended-stopband microstrip lowpass filter using rat-race directional coupler," *Electron. Lett.*, Vol. 49, No. 4, 272–274, 2013.
8. Li, J. L., S. W. Qu, and Q. Xue, "Compact microstrip lowpass filter with sharp roll-off and wide stop-band," *IEE Electron. Lett.*, Vol. 45, No. 2, 110–111, Jun. 2009.
9. Wang, J., H. Cui, and G. Zhang, "Design of compact microstrip lowpass filter with ultra-wide stopband," *IEE Electron. Lett.*, Vol. 48, No. 14, 854–856, Jul. 2012.
10. Abdipour, A., Ar. Abdipour, and S. Lotfi, "A lowpass filter with sharp roll-off and high relative stopband bandwidth using asymmetric high-low impedance patches," *Radioengineering*, Vol. 24, No. 3, 712–716, 2015.
11. Wei, F., L. Chen, X.-W. Shi, Q.-L. Huang, and X.-H. Wang, "Compact lowpass filter with wide stop-band using coupled-line hairpin unit," *Electron. Lett.*, Vol. 46, No. 1, 88–90, 2010.
12. Ma, K. and K. S. Yeo, "New ultra-wide stopband low-pass filter using transformed radial stubs," *IEEE Trans. Microw. Theory. Tech.*, Vol. 59, No. 3, 604–611, Mar. 2011.
13. Nouritabar, A. R., A. Abdipour, and Ar. Abdipour, "A design of low-pass filter with wide stopband and sharp roll-off rate using series LC tanks resonator," *Applied Computational Electromagnetics Society (ACES) Journal*, Vol. 31, No. 11, 1343–1350, 2016.
14. Abdipour, Ar. and A. Abdipour, "Compact microstrip lowpass filter with an ultra-wide stopbandand sharp transition band using T-shaped and polygon resonators," *Progress In Electromagnetics Research C*, Vol. 74, 51–61, 2017.
15. Abdipour, A., Ar. Abdipour, and F. Lorestani, "A compact microstrip lowpass filter with sharp roll-off rate and ultra-wide stopband employing coupled polygon patches," *Progress In Electromagnetics Research C*, Vol. 76, 171–183, Aug. 2017.
16. Hong, J.-S. and M. J. Lancaster, *Microstrip Filters for RF/Microwave Applications*, John Wiley & Sons, Inc., 2001.